J Mater Sci (2026) 61:22852–22871

Electronic materials

Enhancing optical and electrical properties of PVA/PVP–GnP nanocomposites for advanced applications

Ömer Bahadır Mergen[1,*] and Ertan Arda[2]

[1] *Department of Medical Imaging Techniques, Dokuz Eylul University, Izmir, Turkey*
[2] *Department of Physics, Faculty of Science, Trakya University, Edirne, Turkey*

Received: 28 August 2025
Accepted: 8 June 2026
Published online: 22 June 2026

© The Author(s), 2026

ABSTRACT

The aim of this study is to investigate the synthesis and comprehensive characterization of Polyvinyl alcohol/Polyvinylpyrrolidone-Graphene nanoplatelet (PVA/PVP–GnP) nanocomposite films prepared using the solution mixing method. The structural, electrical, and optical properties of the films were evaluated, revealing significant enhancements in their physical properties attributed to the incorporation of GnPs. Electrical conductivity values dramatically increased from 1.96×10^{-10} (for the pure PVA/PVP hybrid matrix) to 4.07 S m^{-1} (for the composite with 6.16 vol% GnP), due to the formation of conductive pathways created by the GnP network. Optical analysis demonstrated strong UV absorption, with a notable decrease in optical bandgap energy as GnP concentration increased, related to the creation of new localized energy states and charge transfer complexes. The Urbach energy, indicative of structural disorder and defect density, also increased with higher GnP content, reflecting enhanced electron transitions in the material. Refractive index, optical conductivity, and dielectric properties showed significant improvements, further supporting the potential of these materials for optoelectronic and photonic applications. The results emphasize the versatility of these nanocomposites for energy storage systems and other high-performance applications.

Handling Editor: Yao Zhou.

Address correspondence to E-mail: bahadir.mergen@deu.edu.tr

https://doi.org/10.1007/s10853-026-13182-0

GRAPHICAL ABSTRACT

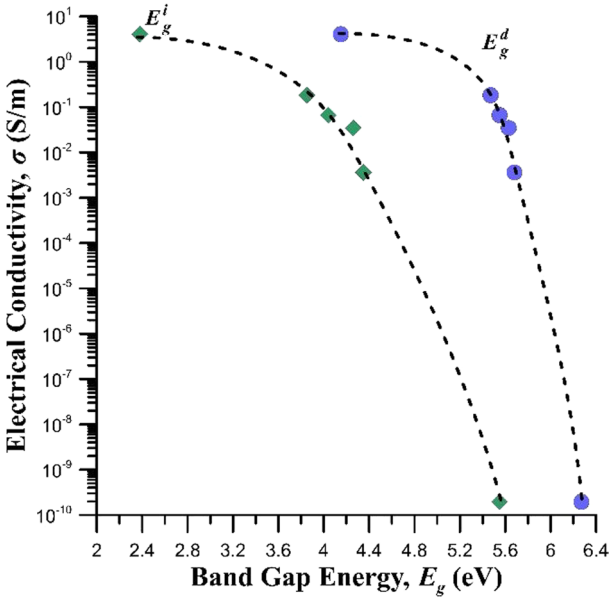

Introduction

Polymeric nanocomposites have become a significant area of research in recent years due to their unique mechanical, electrical, thermal, and optical properties. These materials are widely used in various applications, ranging from optical and optoelectronic devices to drug delivery systems, owing to their biocompatibility, low cost, and ease of accessibility [1]. The development of nanocomposites is achieved by incorporating various nanomaterials into a polymer matrix, which enhances mechanical strength while maintaining the lightweight nature of the polymer and addressing its inherent limitations [2]. Moreover, the physicochemical advantages offered by nanomaterials—such as high surface area and reactivity—have broadened their application in energy conversion systems, including photovoltaic devices, sensors, and photonic technologies [3]. Due to their ease of production and environmental stability, polymeric nanocomposites stand out as promising candidates for the development of sustainable and high-performance materials [3].

Polyvinylpyrrolidone (PVP) and polyvinyl alcohol (PVA) are considered ideal polymers for numerous technological applications owing to their biocompatibility, water solubility, and non-toxic nature [1]. Particularly, PVA exhibits excellent film-forming properties due to its semi-crystalline structure and ability to form hydrogen bonds, while the amorphous structure of PVP enhances the homogeneous distribution of additives, strengthening the stability of the polymer matrix [1, 4]. The blending of these two polymers enables the development of hybrid systems with improved mechanical, optical, and functional properties suitable for optoelectronic devices, sensors, and biomedical applications [5]. Furthermore, the hydrophilic nature and reactive functional groups of PVA allow easy crosslinking with dopants, while the high polarity and dielectric constant of PVP make it an excellent additive for solar cells, flexible coatings, and biomedical devices [6, 7].

Ongoing research in polymeric nanocomposites has reinforced the trend of blending different polymers to improve material performance and enable new applications. The scientific community is focusing on the development of hybrid polymer nanocomposites for diverse applications such as water purification, energy storage, sensing, and solar energy harvesting [4]. The solution casting method is widely preferred for preparing thin films, as it allows for homogeneous dispersion and enables the controlled combination of different polymers to produce materials with superior physical and chemical properties [4, 5]. These hybrid structures surpass the physical capabilities of materials composed of a single polymer type, enabling the design of more durable and functional systems [8]. In

recent years, polymer blends have emerged as a strategic approach in technological device development, gradually replacing single-component polymers to yield more efficient and innovative materials [6].

Although PVA and PVP can be used in various applications, their inherent limitations restrict their performance in some cases. PVA suffers from low thermal stability and high water absorption capacity, which can reduce its mechanical strength and structural integrity, particularly under humid conditions [5]. Its low refractive index also limits its potential in optoelectronic applications [7]. PVP, on the other hand, has a brittle structure and limited mechanical strength, making it less suitable for flexible device fabrication [6]. Furthermore, both polymers exhibit low electrical conductivity, which hinders their use in electronic and energy storage applications [9]. To address these drawbacks, conductive fillers—especially carbon-based materials such as graphene and carbon nanotubes—are frequently incorporated. These fillers provide superior electrical conductivity, large surface area, and chemical stability, significantly improving the electrical, mechanical, and thermal performance of polymer composites [9]. However, ensuring compatibility between these nanomaterials and polymer matrices, achieving homogeneous dispersion, and preventing agglomeration remain major engineering challenges [2]. In polymer nanocomposites, the degree of nanoparticle–polymer interaction and the surface area of the filler are decisive factors governing the overall material properties [8].

In this context, the PVA/PVP blend has gained significant attention as a versatile and tunable host matrix for nanocomposites. The high miscibility of PVA and PVP arises from the strong hydrogen bonding between the hydroxyl (–OH) groups of PVA and the carbonyl (C=O) groups of PVP [10–12]. These interactions enhance the structural homogeneity and physicochemical stability of the blend. Studies have demonstrated that PVA and PVP form a thermodynamically miscible pair at all composition ratios [10, 13]. Both polymers are water-soluble and biocompatible, facilitating the preparation of homogeneous hybrid matrices and their modification with conductive nanofillers such as graphene nanoplatelets (GnP) [14–16]. The semicrystalline nature of PVA provides mechanical strength, while the amorphous PVP component reduces crystallinity, improving the optical and structural properties of the material [17–19]. Moreover, PVP decreases the crystalline phase of PVA, imparting flexibility and amorphousness, whereas PVA acts as a plasticizer for PVP [20]. The synergistic combination of these polymers enhances optical transparency and electrical conductivity. The hydrogen bonding between PVA and PVP chains also enables strong interfacial interactions with nanofillers such as GnP [16, 21]. Consequently, the PVA/PVP matrix serves as an ideal platform for developing GnP-based nanocomposites with enhanced electrical and optical properties [14, 19, 22].

Graphene nanoplatelets (GnPs) stand out as a cost-effective alternative to single-layer graphene, offering high electrical and thermal conductivity along with excellent mechanical strength [23]. However, it should be noted that the optical and electrical properties of GnPs may be limited compared to those of single-layer graphene due to their multi-layered structure [24]. Although GnPs possess high specific surface areas, surface modification may sometimes be necessary to ensure adequate interaction with the polymer matrix. Additionally, unlike graphene oxide (GO), GnPs largely retain their optical, electrical, and mechanical properties by preserving their pristine basal plane structure [24]. In recent years, polymer-based nanocomposites have attracted significant interest across a wide range of applications—from optical filters to biosensors, and from fuel cells to high-performance dielectric materials [7]. The flexible nature of polymers makes them a suitable matrix for various nanomaterials, while the careful selection and dispersion of nanofillers enable the optimization of material properties. In this context, various factors—such as the shape, size, and concentration of nanoparticles—have been strategically utilized to enhance the optical, mechanical, and electrical performance of polymer nanocomposites [25].

Alsaif et al. [3] demonstrated that polyvinyl alcohol/manganese dioxide (PVA/MnO_2) nanomaterials could be useful in high-performance optoelectronic devices. Badawi and Alharthi [1] investigated the linear and nonlinear optical and electrical properties of reduced graphene oxide/cobalt-doped titanium dioxide (rGO/Co:TiO_2)-doped PVP/PVA nanocomposites, demonstrating their potential for effective integration into optoelectronic applications. In another study, incorporating Sb_2S_3 chalcogenide nanopowder into the PVA/PVP hybrid matrix was shown to significantly enhance the optical properties [5]. Mohamed et al. [26] focused on determining the optimal doping levels in poly(vinyl alcohol)/poly(vinyl pyrrolidone)/

(polyethylene glycol)/zinc tungstate/polyaniline (PVA/PVP/PEG/$ZnWO_4$/PANi) nanocomposites for use in optoelectronic and energy storage applications. Similarly, Soliman et al. [7] proposed the use of PVA/Bi-Ni oxide-rGO nanocomposites in optical device applications by enhancing their optical properties.

This study aims to determine the structural, optical, and electrical properties of PVA/PVP hybrid matrix nanocomposites incorporating graphene nanoplatelets (GnPs). The primary objective is to investigate the effect of different GnP concentrations (0.00, 1.19, 2.40, 3.63, 4.88, and 6.16 vol%) on the performance of the hybrid nanocomposites and to evaluate their potential for optical energy storage devices and optoelectronic applications. Electrical conductivity measurements demonstrated a significant enhancement in conductivity with increasing GnP content. The optical bandgap (E_g) exhibited a decreasing trend, while the Urbach energy (E_u) increased, indicating higher disorder levels in the material. The improved structural, optical, and electrical characteristics of PVA/PVP–GnP nanocomposites underscore their potential for high-performance applications in optoelectronics, energy storage, and photonic technologies.

Material and method

Polyvinyl alcohol (PVA, P8136, Sigma-Aldrich) with a density of 1.19–1.31 g cm^{-3}, melting point of 250 °C, viscosity of 4–6 cP (4% in H_2O at 20 °C, lit.), average molecular weight of 30,000–70,000, and a hydrolysis degree of approximately 87–90% was used. Polyvinylpyrrolidone (PVP K30, 81,420, Sigma-Aldrich) with a pH of 5.0–8.0 (10 g/L at 20 °C) and a density of 1.20 g cm^{-3} was also employed. Graphene nanoplatelets (GnP, 900413, Sigma-Aldrich) possessing an oxygen content below 1%, a specific surface area of 120–150 m^2 g^{-1}, an average thickness of 6–8 nm, a particle size of 25 μm, a melting point of 3652 °C, and a density of 2.2 g cm^{-3} were obtained from Sigma-Aldrich. All material specifications were obtained from the manufacturer's technical data sheets available on the official Sigma-Aldrich website.

For the preparation of PVA/PVP (80/20 wt%)–GnP nanocomposite dispersions, 1.92 g of PVA and 0.48 g of PVP powders were first dissolved separately in 30 mL of double-distilled water at 70 °C under magnetic stirring until complete dissolution was achieved. Stirring was continued until the solutions cooled to room temperature. The obtained solutions were then combined under magnetic stirring to form a homogeneous PVA/PVP hybrid polymer stock solution. Subsequently, this homogeneous solution was divided into six smaller vials, into which varying amounts of GnP, determined according to the equation given below, were added.

$$\phi = \frac{m_{GnP}/\rho_{GnP}}{m_{GnP}/\rho_{GnP} + m_{PVA}/\rho_{PVA} + m_{PVP}/\rho_{PVP}} \quad (1)$$

where, m_{PVA}, m_{PVP}, and m_{GnP} are the mass, ρ_{PVA}, ρ_{PVP} and ρ_{GnP} are the density of the PVA, PVP, and GnP in the nanocomposite dispersions, respectively. To ensure the homogeneous dispersion of GnPs within the PVA/PVP matrix, the mixtures were magnetically stirred every 6 h at room temperature using a multi-position magnetic stirrer and subsequently subjected to sonication for 10 min. This process was continued for a total of 48 h at room temperature. The obtained homogeneous pure PVA/PVP and PVA/PVP–GnP mixtures were then cast into films using the solution casting method. The PVA/PVP–GnP dispersions were dropped onto 2.5 × 2.5 cm^2 quartz glasses substrates and then dried at room temperature for 2 days until no residual solution or cracks remained in the hybrid nanocomposites. The images of the produced pure PVA/PVP hybrid matrix and PVA/PVP–GnP nanocomposite films are presented in Fig. S1. Using Eq. (1), the volume fractions (ϕ) of the samples were determined as 0.00, 1.19, 2.40, 3.63, 4.88 and 6.16 vol%.

All measurements were performed using three identical nanocomposite films for each ϕ value. During the measurements, the laboratory temperature was maintained at 24–25 °C and relative humidity of 55–60%. The electrical conductivities of the PVA/PVP–GnP nanocomposites were measured using a Keithley 6517A electrometer, which complies with the ASTM-D257 standard and employs alternating polarity method. A Varian Cary 100 Bio Model UV–Visible spectrometer, fabricated by Varian Instruments, Australia, was used to determine the UV–Vis absorbance and reflectance spectra in the wavelength range of 190 to 600 nm. The FTIR spectra of the samples were obtained using a Perkin Elmer Frontier spectrometer within the wavenumber range of 4000–500 cm^{-1}, aiming to determine the characteristic functional groups and potential interactions between the polymer matrix and the incorporated nanofillers. The surface morphology of the PVA/PVP hybrid matrix and the PVA/PVP–GnP nanocomposite films was examined

using a scanning electron microscope (Thermo Scientific Scios 2 DualBeam).

The absorption coefficient (α) [27] and the extinction coefficient (k) [28] were calculated using Eqs. 2 and 3, respectively.

$$\alpha = \frac{(2.303)A}{d} \tag{2}$$

$$k = \frac{\alpha\lambda}{4\pi} \tag{3}$$

where d is the film thickness, A is the absorbance, and λ is the wavelength.

The optical band gap (E_g) values of the nanocomposites were calculated using the Tauc method (Eq. 4) [29] and the ASF methods (Eqs. 5 and 6) [30].

$$\alpha h\nu = B\left(h\nu - E_g\right)^m \tag{4}$$

$$A = C\lambda\left[\frac{1}{\lambda} - \frac{1}{\lambda_g}\right]^m + D \tag{5}$$

$$E_g = \frac{1239.83}{\lambda_g} \tag{6}$$

Here α, $h\nu$, A, λ, λ_g, B, C, and D represent the absorption coefficient, the photon energy of the incident light, absorbance, wavelength, the wavelength corresponding to the optical band gap energy, and constants, respectively. The type of electronic transition depends on the parameter m in Eqs. (4) and (5), where $m = 0.5$ corresponds to allowed direct transitions, and $m = 2$ corresponds to allowed indirect transitions.

The Urbach energy (E_u) [31], refractive index (n) [32], optical conductivity (σ_{opt}) [32, 33], and the complex dielectric constant of the material (ε), including its real part (ε_r) and imaginary part (ε_i) [32], were determined as follows:

$$\alpha = \alpha_0 \exp\left(\frac{h\nu}{E_u}\right) \tag{7}$$

$$A = F\exp\left(\frac{hc}{E_u\lambda}\right) \tag{8}$$

$$n = \left(\frac{1+R}{1-R}\right) + \sqrt{\frac{4R}{(1-R)^2} - k^2} \tag{9}$$

$$\sigma_{opt} = \frac{\alpha nc}{4\pi} \tag{10}$$

$$\varepsilon = \varepsilon_r + i\varepsilon_i \tag{11}$$

$$\varepsilon_r = n^2 - k^2, and \varepsilon_i = 2nk \tag{12}$$

Here α_0 is a pre-exponential constant, h is the Planck constant, ν is the frequency, c is the speed of light, λ is the wavelength, R is the reflectance, k is the extinction coefficient, α is the absorption coefficient, and F is a constant.

The energy dispersion performance of the nanocomposites was analyzed using the Wemple–DiDomenico (WDD) model (Eq. 13) [26, 33–35]. Additionally, the W–D model allows the determination of other optical constants of the material, such as the static refractive index (n∞), static dielectric constant (ε_s), and oscillator strength (f) [33, 36, 37]. The Sellmeier oscillator model [36, 38] was applied to determine the average oscillator strength (S_o) and the average oscillator wavelength (λ_o).

$$\frac{1}{n^2-1} = \frac{E_o}{E_d} - \frac{1}{E_oE_d}(h\nu)^2 \tag{13}$$

$$n_o = \left(1 + \frac{E_d}{E_o}\right)^{1/2} \tag{14}$$

$$\varepsilon_s = \left(n_\infty\right)^2 \tag{15}$$

$$f = E_dE_o \tag{16}$$

$$\frac{n_\infty^2 - 1}{n^2 - 1} = 1 - \left(\frac{\lambda_o}{\lambda}\right)^2 \tag{17}$$

$$\left(n^2-1\right)^{-1} = \frac{1}{S_o\lambda_o^2} - \frac{1}{S_o}\lambda^{-2} \tag{18}$$

$$S_o = \frac{n_\infty^2 - 1}{\lambda_o^2} \tag{19}$$

Using the Spitzer–Fan model [39] and the Drude free electron model [34], the dielectric constant at short wavelengths (ε_l), the free carrier concentration to effective mass ratio (N/m^*), relaxation time (τ), optical electronic mobility (μ_{opt}), and resonant

plasma frequency (ω_p) of the nanocomposites were obtained.

$$\varepsilon_r = n^2 - k^2 = \varepsilon_l - \left(\frac{e^2}{4\pi^2 c^2 \varepsilon_o}\frac{N}{m^*}\right)\lambda^2 \quad (20)$$

$$\varepsilon_i = J\left(\frac{1}{\tau}\right)\lambda^3, \quad J = \frac{e^2}{8\pi^3 c^3 \varepsilon_o}\frac{N}{m^*} \quad (21)$$

$$\mu_{opt} = \frac{e\tau}{m^*} \quad (22)$$

$$\omega_p = \frac{e^2 N}{\varepsilon_o m^*} \quad (23)$$

Here ε_l, e, c, ε_o, and N/m^* represent the dielectric constant at short wavelengths, the electron charge, the speed of light, the permittivity of free space, and the ratio of charge carrier density (N) to the effective mass (m^*), respectively.

Results and discussion

Scanning electron microscopy (SEM) analysis of the nanocomposites

The SEM images of the PVA/PVP hybrid matrix and the PVA/PVP–GnP nanocomposites are presented in Fig. 1. The images show that the PVA/PVP hybrid matrix film exhibits a typically homogeneous polymer-blend morphology. In Fig. 1a, the surface appears generally smooth, continuous, and free of prominent macropores at a magnification of 10 kx. This morphology indicates a compatible mixing of the polymer chains, supporting the good interaction and phase compatibility between PVA and PVP. The small particulate features and slight protrusions observed locally on the surface may be associated with microscale condensations or local drying effects within the polymer matrix; however, these features are not significant enough to compromise the integrity of the structure. At a higher magnification of 50 kx Fig. 1b, the matrix exhibits a compact, dense, and non-porous microstructure, with no evident phase separation—consistent with the high miscibility of PVA and PVP. The surface roughness is also observed to be on the nano- to microscale. In Fig. 1c, the platelet-like structures embedded within the PVA/PVP hybrid matrix are not strongly pronounced, indicating that the GnP sheets are well dispersed. The absence of distinct gaps or large voids at the polymer–filler interface suggests good interfacial interaction between the matrix and the GnP. Figure 1d shows that, with increasing GnP content, a larger number of GnP platelets become visible, randomly distributed and in contact with one another. The morphology and distribution of the GnP sheets play a significant role in influencing the physical properties of the nanocomposite.

FTIR analysis of the nanocomposites

The FTIR spectra of the pure PVA/PVP hybrid matrix and PVA/PVP–GnP nanocomposites were examined to determine the chemical interactions between the polymer matrix and the filler Fig. 2. The pure PVA/PVP blend exhibits a weak O–H stretching peak around 3674 cm^{-1} and a broad hydroxyl band in the range of 3584–3060 cm^{-1}. This broad band reflects the strong hydrogen bonding between the hydroxyl (–OH) groups of PVA and the carbonyl (C=O) groups of PVP [10, 40]. Upon the addition of GnP, a decrease in the bandwidth and a slight shift toward lower wavenumbers were observed, indicating that the filler induces a rearrangement of hydrogen bonds among the polymer chains [1, 14].

Distinct bands observed at 2987 cm^{-1} and 2901 cm^{-1} correspond to the aliphatic C–H stretching vibrations in the PVA and PVP chains [10]. The variation in their intensity suggests that the local environment around the methylene groups changes due to the physical interactions between GnP and the polymer chains [5]. The sharp band at 1651 cm^{-1} is attributed to the carbonyl (C=O) stretching vibration of PVP and represents a characteristic feature of the PVA/PVP blend. This peak confirms the formation of intermolecular hydrogen bonds between the –OH groups of PVA and the C=O groups of PVP [10, 40]. A slight red shift of the 1651 cm^{-1} band with increasing GnP content indicates that the filler strengthens these interactions and facilitates bonding between polymer chains [1, 14].

The band at 1422 cm^{-1} corresponds to the symmetric bending vibration of CH_2 groups, while those at 1250 cm^{-1} and 1066 cm^{-1} are assigned to C–O–C and C–O stretching vibrations, respectively [12]. In particular, the C–O stretching band near 1066 cm^{-1} shows a slight shift upon GnP incorporation, supporting the presence of weak interactions (such as π–π or van der Waals forces) between the filler and the polymer chains [5, 40]. Additionally, the low-wavenumber

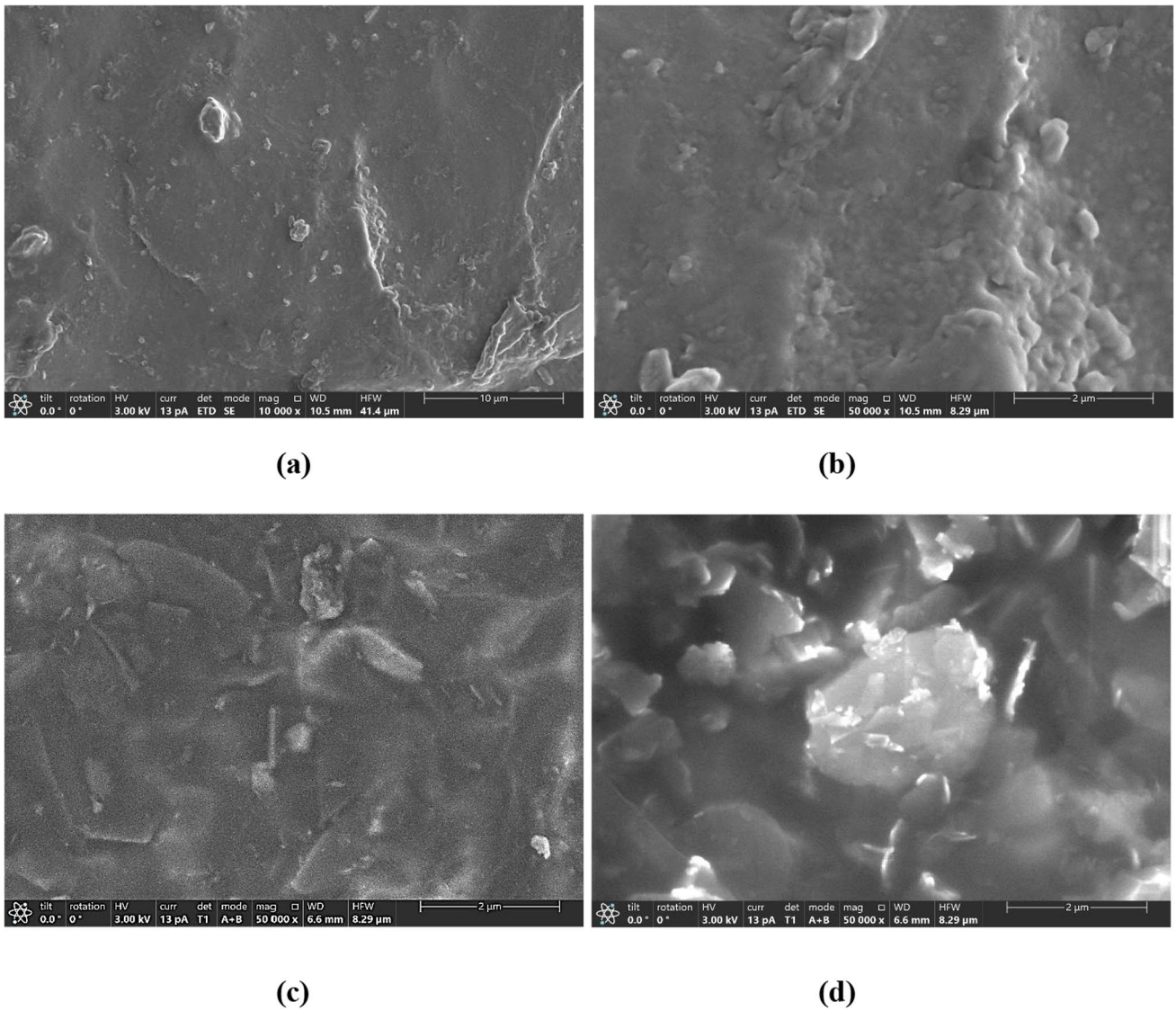

Figure 1 SEM images of the PVA/PVP hybrid matrix at magnifications of **a** 10 k and **b** 50 k, as well as those of the PVA/PVP–GnP nanocomposites with GnP loadings of **c** $\phi = 2.40$ vol% and **d** $\phi = 6.16$ vol%.

bands observed at 772 cm^{-1} and 648 cm^{-1} are associated with C–C vibrations within the polymer backbone [14]. The sharpening of peaks in this region suggests that the highly ordered structure of GnP is successfully integrated into the PVA/PVP matrix.

The obtained FTIR results are in good agreement with those reported in the literature for other PVA/PVP-based nanocomposites [1, 5, 10, 12, 14, 40]. Specifically, the narrowing of the broad O–H band, the slight shift in the C=O stretching peak, and the changes in C–O vibrations indicate strong physical interactions between GnP and the polymer chains. These findings confirm that GnP exhibits good compatibility and strong interfacial interactions with the PVA/PVP matrix, thereby enhancing the structural integrity and homogeneity of the nanocomposite.

Electrical conductivity of the nanocomposites

The measured electrical conductivity value is approximately 1.96×10^{-10} S m^{-1} for the pure PVA/PVP hybrid matrix, increasing to 4.07 S m^{-1} for the PVA/PVP–GnP film with 6.16 vol% GnP as listed in Table 1. The addition of GnPs to PVA/PVP hybrid matrix significantly increases the electrical conductivity of the resulting composite material. This is because the electrical

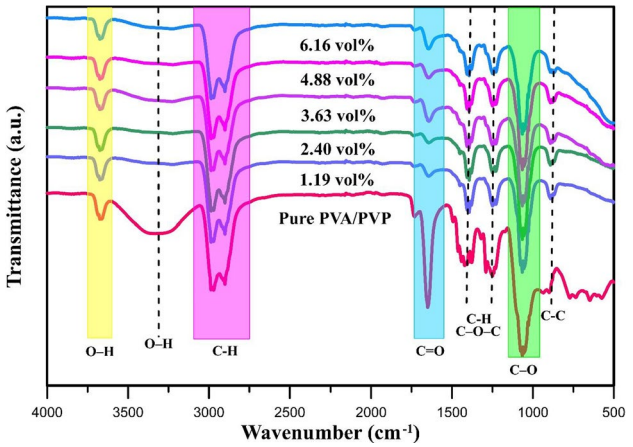

Figure 2 The FTIR spectra of pure PVA/PVP hybrid matrix and PVA/PVP–GnP nanocomposite films.

conductivity of GnPs is much higher than that of the PVA/PVP hybrid matrix. When GnPs are dispersed in the PVA/PVP matrix, they form an interconnected network of conductive pathways, leading to an increase in the conductivity of the composite. Consequently, the PVA/PVP–GnP nanocomposites exhibit higher conductivity than the pure PVA/PVP hybrid matrix.

UV–Vis analysis of the nanocomposites

UV–Vis absorption spectra, which provide detailed information about the optical behavior, optical parameters, and electronic band structures of materials, are very useful for investigating crystalline and amorphous polymeric materials [41, 42]. The absorbance (A) values of all nanocomposite samples measured in the wavelength range of 190–600 nm are presented in Fig. S2a. The pure PVA/PVP hybrid matrix exhibits low absorbance values across this range, indicating its transparency. All PVA/PVP–GnP samples show strong absorption in the 190–250 nm wavelength range, while absorbance remains nearly constant across the 250–600 nm range. The figure shows that absorbance increases below 250 nm for all film samples. Additionally, a strong absorbance peak associated with the $\pi \rightarrow \pi^*$ transition appears at approximately 190 nm [4, 9]. As the GnP content in the composites increases, an absorbance peak around 260 nm becomes more pronounced. This small increase is attributed to GnPs in the composite structure acting as photon scattering centers. The figure also reveals that increasing the amount of GnP in the composites leads to higher absorbance levels.

The absorption coefficient (α) is often used to characterize the absorption of light in various materials. It is particularly useful for comparing materials of different thicknesses. The variation of absorption coefficient with wavelength for all samples is shown in Fig. 3. As can be seen from the figure, the absorption coefficient follow a similar trend to absorbance data. As the amount of GnP increases in the nanocomposite samples, the absorption coefficient values gradually increase in the Vis region and then increase more sharply in the UV region. In other words, as the doping level in the composite material increases, the absorption of light in the UV region correspondingly increases.

The extinction coefficient (k), which represents the amount of energy lost due to light scattering and absorption in a material, defines the likelihood of electronic transitions within the material and is highly important for various optical and photonic applications [43, 44]. The variation of the extinction coefficient with wavelength for all samples is presented in Fig. S2b. It can be seen from the figure that as the wavelength decreases from higher values (visible region) to lower values (UV region), the extinction coefficient (k) initially exhibits a linear downward trend, followed by a noticeable increase in the range

Table 1 Electrical conductivity (σ), Refractive index (n), Urbach energy (E_u) and optical band gap energies (E_g^d and E_g^i) obtained with Tauc and ASF methods for pure PVA/PVP and PVA/PVP–GnP nanocomposites

ϕ (vol.%)	σ (S m^{-1})	N (at 400 nm)	Tauc method			ASF method		
			E_g^d(eV)	E_g^i(eV)	E_u (eV)	E_g^d(eV)	E_g^i(eV)	E_u (eV)
0.00	1.96×10^{-10}	1.85	6.3	5.6	0.84	6.3	5.6	0.84
1.19	3.65×10^{-3}	1.88	5.7	4.4	0.95	5.7	4.4	0.95
2.40	3.47×10^{-2}	1.96	5.6	4.3	1.04	5.6	4.3	1.04
3.63	6.66×10^{-2}	2.00	5.6	4.0	1.20	5.6	4.0	1.20
4.88	1.83×10^{-1}	2.10	5.5	3.9	1.23	5.5	3.9	1.23
6.16	4.07	2.22	4.2	2.4	2.56	4.2	2.4	2.56

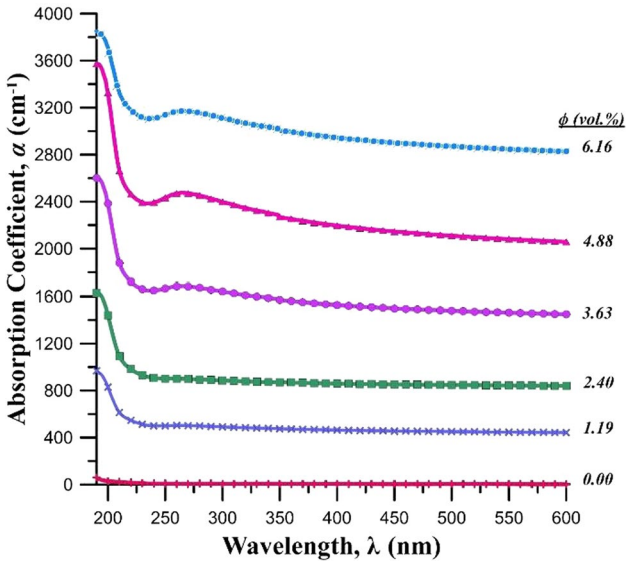

Figure 3 The absorption coefficient (α) spectra of pure PVA/PVP hybrid matrix and PVA/PVP-GnP nanocomposite films.

of 190–220 nm. This behavior is consistent with our previous findings reported in Mergen et al. [42]. As the volume fraction of the GnP filler in the composite increases, the absorption coefficient values increase accordingly, leading to greater energy loss [30]. Higher GnP doping in the PVA/PVP hybrid results in a significant increase in both the absorption and extinction coefficient values. In other words, the nanocomposites exhibit an enhanced capacity to absorb and dissipate electromagnetic energy, indicating that both absorption and extinction properties improve with increasing GnP concentration.

Determination of optical band gap energy

The energy difference between the highest occupied molecular orbital (HOMO) and the lowest unoccupied molecular orbital (LUMO) is defined as the optical band gap (E_g) [42]. Determining the optical band gap energy of semiconductor polymer composites is critical for many applications. One common method to determine E_g involves analyzing the absorption spectrum, as its high-energy region provides insights into electronic transitions. The optical band gap energy of semiconductors is evidenced by an increase in absorbance at a specific wavelength.

The increase observed in the absorption coefficient (α) values for wavelengths between 190 and 230 nm in Fig. 3 indicates that the photons within this range possess sufficient energy to excite electrons from the valence band to the conduction band in the nanocomposite material [45]. Tauc plots for all the samples are shown in Fig. 4a, b, corresponding to allowed direct transitions and allowed indirect transitions, respectively. The E_g values were obtained by extrapolating the linear portion of the Tauc graph to the $h\nu$ axis and are listed in Table 1.

One common source of error in determining E_g is inaccurate measurement of the film thickness. This can lead to imprecise calculation of the absorption coefficient when using the Tauc method. To eliminate this thickness effect, Absorption Spectrum Fitting (ASF) method can be used, where absorption data is used instead of absorption coefficient. According to Eq. 5, the $\left(A\lambda^{-1}\right)^{\frac{1}{m}}$ versus λ^{-1} graphs for direct and indirect transitions are plotted in Fig. S3a, b, respectively. The λ_g values were determined by extrapolating the linear region to the λ^{-1} axis, as shown in Fig. S3a, b. The band gap energies corresponding to λ_g were calculated using Eq. 6 and are presented in Table 1.

In our previous studies, we demonstrated that increasing the carbon filler content reduced the E_g^d from 5.90 to 5.16 eV and the E_g^i from 5.33 to 2.63 eV in PVA/CS/MWCNT biocomposites, while in PVP/GnP nanocomposites, the E_g^d decreased from 5.51 to 3.89 eV and the E_g^i from 5.19 to an average of 1.63 eV [30, 42]. Similarly, in the present study, the effect of GnP incorporated into the hybrid PVA/PVP matrix on the optical band gap has been clearly observed.

As shown in Table 1, the E_g values obtained from both the Tauc and ASF methods are identical. For the pure PVA/PVP hybrid matrix, the direct band gap energy was determined as $E_g^d = 6.27$ eV, and the indirect band gap energy as $E_g^i = 5.55$ eV using both methods. As the GnP content increased in the samples, the calculated optical band gap energies decreased due to the formation of new energy states. For the sample with $\phi = 6.16$ vol% GnP, band gap energies were calculated as $E_g^d = 4.15$ eV and $E_g^i = 2.38$ eV. This decrease in optical band gap energy results from the presence of GnPs in the composite structure, which form charge transfer complexes and create new localized energy states [32]. Additionally, the variation of electrical conductivity with optical band gap energy for all the samples is presented in Fig. 5. The graph shows that the

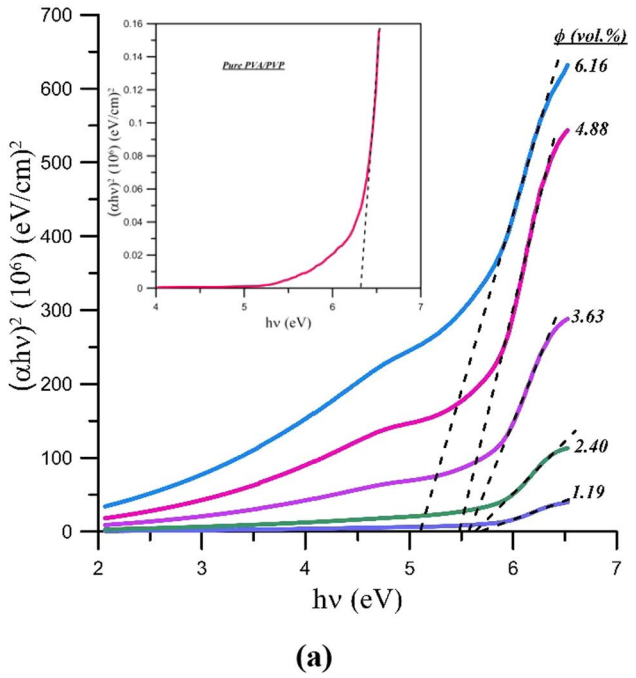

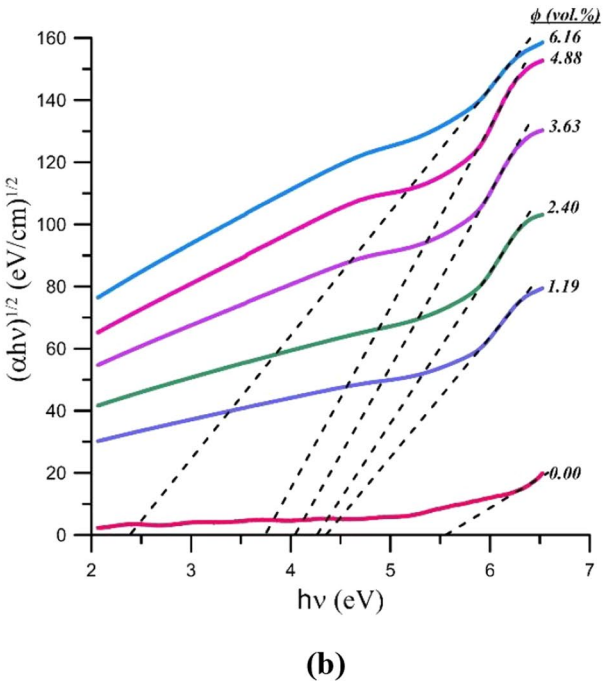

Figure 4 **a** $(\alpha h\nu)^2$ versus $(h\nu)$ plot and **b** $(\alpha h\nu)^{1/2}$ versus $(h\nu)$ plot of pure PVA/PVP hybrid matrix and PVA/PVP–GnP nanocomposites.

addition of GnPs to the pure PVA/PVP hybrid matrix significantly increases electrical conductivity by

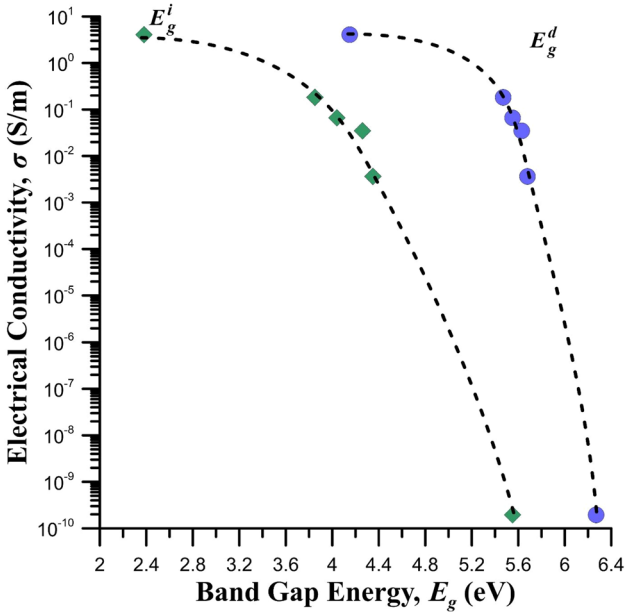

Figure 5 Electrical conductivity (σ) of PVA/PVP–GnP nanocomposites versus optical band gap energies ($E_g^{\,d}$ *and* $E_g^{\,i}$).

increasing the charge carrier density and reduces the optical band gap energy in the nanocomposites.

Determination of Urbach energy

The Urbach energy (E_u) is an important parameter that depends on the level of disorder and defects in the band structure of materials. This energy is associated with the width of localized states at the band edges and represents the Urbach tail, which exhibits an exponential behavior in the optical absorption spectrum of the material [30]. Moreover, Urbach energy is used to examine structural defects and analyze localized electronic states within the material [41]. Urbach analysis is crucial for optimizing the performance of photovoltaic, optoelectronic, and semiconductor devices. The Urbach energies (E_u) of all the PVA/PVP samples were calculated as the inverse of the slope of the linear relationship between *ln(α)* and photon energy *(hν)* as shown in Fig. 6a and are listed in Table 1.

According to the ASF method, Urbach energy (E_u) values of PVA/PVP–GnP nanocomposites were calculated from the slope of the linear region in the *ln(A)* versus *(1/λ)* plots (see Fig. 6b), using the formula $E_u = 1239.83/\text{slope}$. The results are summarized in Table 1. For each volume fraction, Table 1 demonstrates that the Urbach energy (E_u) values obtained from the Tauc and ASF methods are identical. The

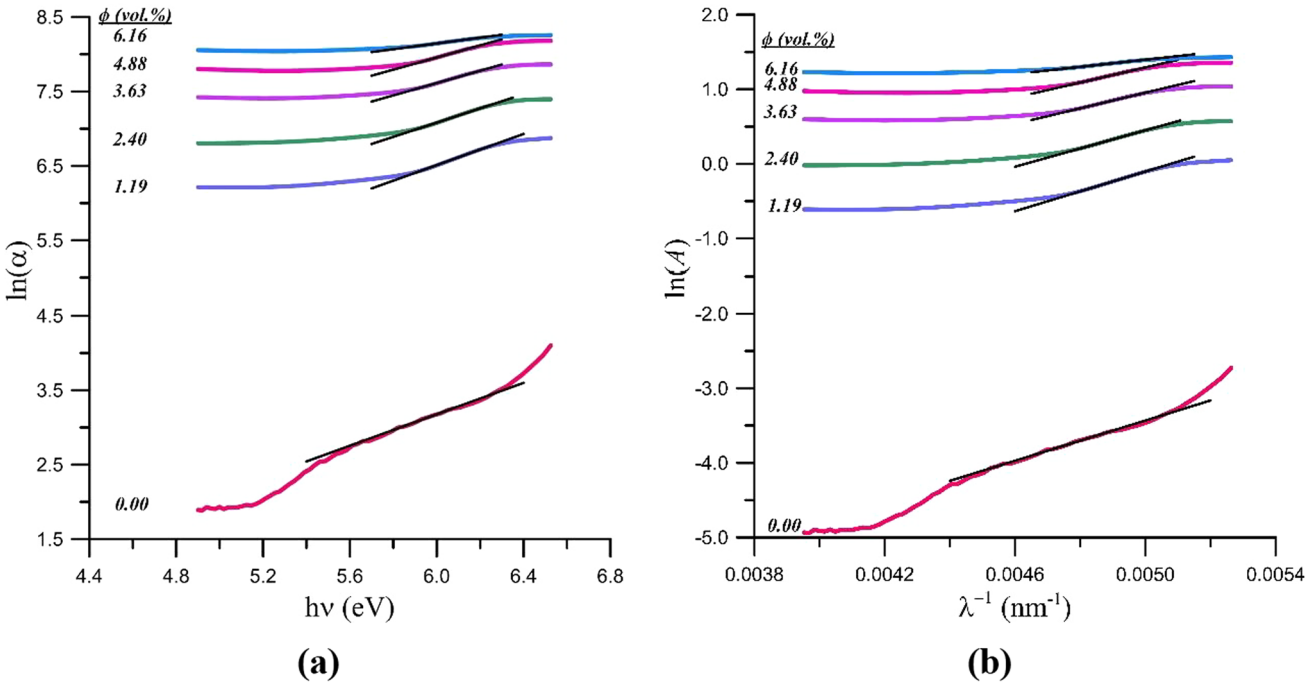

Figure 6 **a** (ln α) versus ($h\nu$) plots **b** (ln A) versus (λ^{-1}) plots of pure PVA/PVP hybrid matrix and PVA/PVP-GnP nanocomposites.

Urbach energy (E_u) value for the pure PVA/PVP hybrid matrix was calculated as 0.84 eV. However, as the GnP content in the hybrid structure increases, the E_u value increases and reaches up to 2.56 eV. These results show that the increase in GnP content within the PVA/PVP hybrid matrix enhances the degree of disorder and defect levels, leading to the formation of localized states in the forbidden band, which facilitates electron transitions [45].

In our previous work on PVP/GnP nanocomposites, we reported that the E_u increased dramatically from 0.13 to 11.48 eV [30]. This pronounced increase was attributed to the more significant structural disorder and interfacial charge trapping sites induced by GnPs within the PVP matrix. In contrast, the variation in Urbach energy observed in the PVA/PVP–GnP nanocomposites progresses in a more controlled and moderate manner. This behavior can be explained by the PVA/PVP hybrid polymer matrix providing a more balanced dispersion environment. Additionally, the hydrophilic nature of PVA may have helped limit the agglomeration of GnP layers, thereby reducing structural disorder.

Reflectance (R) and refractive index (n)

The optical reflection spectra of all samples are presented in Fig. 7a. In the visible region (350–600 nm), the reflectance values remain relatively stable for all compositions, indicating that the incorporation of GnPs does not significantly alter the optical response in this wavelength range. In contrast, a pronounced reflection maximum is observed in the ultraviolet region, centered at approximately 250 nm, which is consistent with the characteristic electronic transitions associated with the graphitic structure of GnPs [32, 46]. As clearly seen in the figure, the intensity of this UV reflection peak systematically increases with increasing GnP content in the PVA/PVP matrix. This behavior suggests that the graphitic nanoplatelets introduce an additional optically active phase, enhancing photon-material interactions at shorter wavelengths. The emergence and amplification of this maximum can be attributed to increased photon scattering and electronic transitions associated with the graphitic structure of GnPs, which become more effective as their volume fraction in the composite

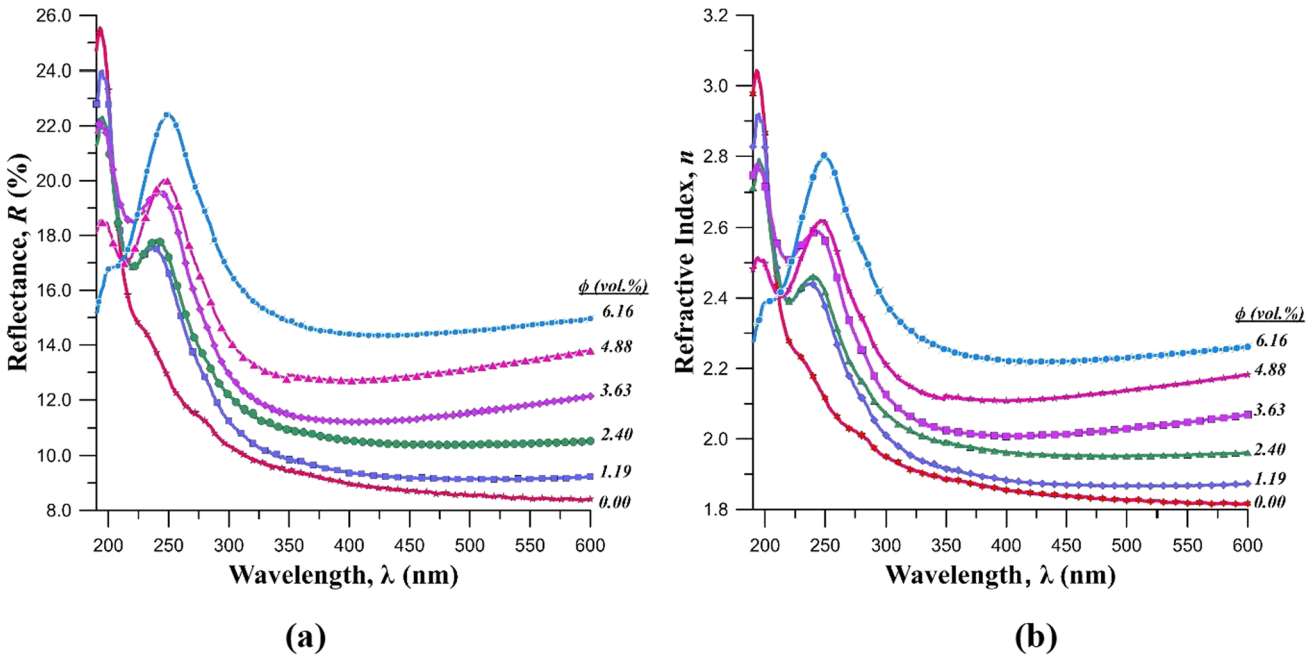

Figure 7 **a** The reflectance (R) and **b** The refractive index (n) spectra versus wavelength (λ) pure PVA/PVP hybrid matrix and PVA/PVP–GnP nanocomposites.

increases. Consequently, all PVA/PVP–GnP nanocomposites exhibit higher reflectance values compared to the pristine PVA/PVP hybrid matrix, with the highest reflectance observed for the sample containing the maximum GnP loading.

The refractive index (n) is a fundamental parameter for evaluating the optical properties of a material and shows the ratio of the speed of light in the vacuum to its speed within the material. This physical parameter is critically important for various applications, including the fabrication of optoelectronic devices, the selection of anti-reflective materials, and the design of optical filters and integrated devices [47, 48]. The refractive index defines the optical properties of a material by affecting light propagation, reflection, and absorbance coefficients. Fillers such as nanoparticles can increase the refractive index by increasing the density of composite films.

The variation of the refractive index values for all samples as a function of wavelength is shown in Fig. 7b. As observed in the figure, the refractive index remains almost constant in the 350–600 nm region for all nanocomposites, but a rapid and significant increase is observed when the wavelength decreases below 350 nm. Notably, the addition of GnP nanoparticles into the PVA/PVP hybrid matrix leads to an increase in the refractive index values of the nanocomposites. The calculated refractive index values for different GnP concentrations at a constant wavelength of 400 nm are given in Table 1.

An increase in filler content within the composite structure alters the internal arrangement of the polymer, leading to an enhancement in the refractive index. This increase is attributed to the changes in filler density and modifications in the polymer matrix structure [47, 49]. The incorporation of GnPs into the hybrid polymer matrix alters the packing density, resulting in variations in refractive index. Furthermore, the addition of GnPs introduces new defect sites within the composite, influencing both the density and polarizability of the material [50, 51]. These structural modifications reduce the transmission of light through the polymer composite, thereby explaining the observed increase in refractive index at higher filler volume fractions [49].

Optical conductivity

The interaction of electromagnetic waves with a material can result in promoting valence electrons to the conduction band. This effect enhances the material's electrical conductivity and optical properties, and is known as photoconductivity which plays a critical role in determining a material's optoelectronic properties

[13, 47]. Optical conductivity (σ_{opt}) defines the material's optical response to electromagnetic waves and is closely associated with interband optical transitions [52]. The reduction of factors such as crystal defects, stress, and lattice deformations improves conductivity, enabling faster propagation of electromagnetic waves and freer movement of electrons within the material [53].

The wavelength-dependent variation in optical conductivity for all samples is shown in Fig. 8. The figure indicates an increase in optical conductivity as the wavelength decreases for all samples. This increase can be attributed to the fact that photons with shorter wavelengths and higher energy are more effective at exciting the material's electrons. As the material absorbs more photons, the absorbance and absorption coefficient increase. Consequently, the optical conductivity rises, as described by Eq. (10). In the low-wavelength region, the photon energy is sufficient to excite electrons from the valence band to the conduction band; as a result, a significant increase in optical conductivity is observed. The addition of GnP nanoparticles into the hybrid matrix increases the density of localized states within the band gap, thereby enhancing both the absorption coefficient and the optical conductivity of the nanocomposites [32]. This enhancement is associated with the formation of charge transfer complexes between GnP and the PVA/PVP hybrid matrix, as well as the increase in the number of free charge carriers due to doping. Furthermore, the decrease in the crystallinity of the polymer films reduces the optical bandgap, contributing to higher optical conductivity. Structural irregularities and the increase in defect states facilitate electron mobility within the band gap, further boosting optical conductivity [13, 24]. The high and stable σ_{opt} values, ranging from 10^{10} to 10^{11} S^{-1}, indicate that the films exhibit a strong photoresponse and hold great potential for applications in optoelectronic devices [51].

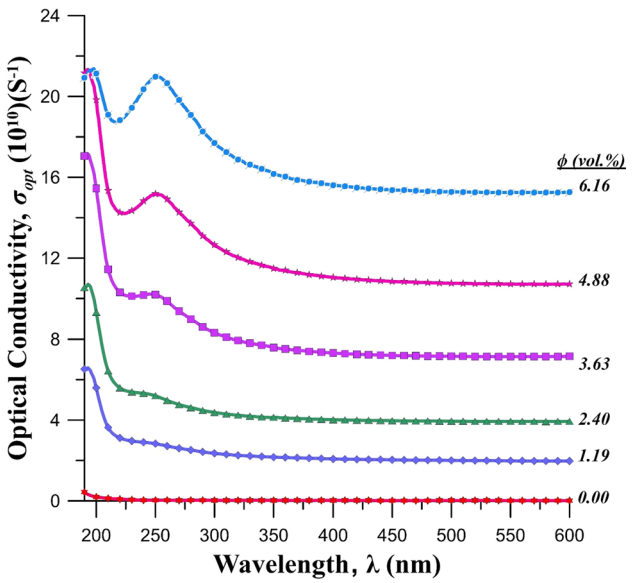

Figure 8 The optical conductivity (σ_{opt}) spectra versus wavelength (λ) for pure PVA/PVP hybrid matrix and PVA/PVP-GnP nanocomposites.

Optical dielectric study

The complex dielectric constant of a material (ε), as given by Eq. (11), consists of two components: the real part (ε_r) and the imaginary part (ε_i), and it serves as a fundamental parameter for understanding a material's response to an electric field [32]. These dielectric components are mathematically related to the values of n and k, as seen in Eq. (12). This constant determines the key optical properties of the material, such as the propagation and absorption of light. Additionally, its frequency dependence plays a critical role in explaining electron excitation processes in polymeric materials. Expressing the electronic density in terms of the complex dielectric constant enables the analysis of the material's interaction with electromagnetic waves [34]. Therefore, identifying materials that can interact with UV–vis radiation and understanding their electronic structure and dielectric properties are crucial for the development of new electronic devices [47].

As shown in Fig. 9a, the variations in the real part of the dielectric constant (ε_r) of all the samples behave similarly to the refractive index. From the figure, it is evident that increasing the GnP content in the hybrid structure significantly enhances the ε_r values. At a wavelength of 400 nm, the ε_r value increases from 3.44 (pure PVA/PVP hybrid matrix) to 4.94 (6.16 vol% PVA/PVP–GnP nanocomposite), indicating enhanced electrical energy storage capacity in the nanocomposites. The variation of the dielectric loss component (ε_i) with wavelength for all the samples is given in Fig. 9b. The spectral behaviors of ε_i and k are quite similar, and both parameters increase significantly with increasing GnP content in the nanocomposites. The decreasing ε_i values at lower wavelengths indicate that PVA/PVP–GnP nanocomposites absorb less electromagnetic energy in that region. Consequently, the interactions between GnP and the PVA/PVP matrix enhance the

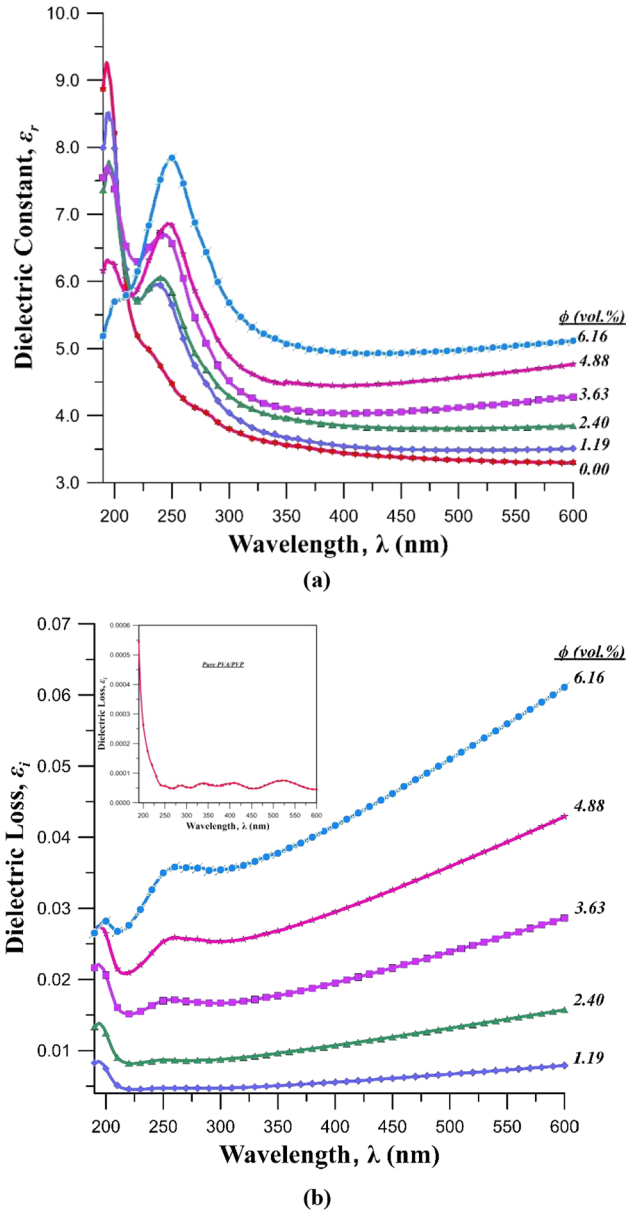

Figure 9 **a** The dielectric constant (εr) and **b** dielectric loss (εi) spectra versus wavelength (λ) for pure PVA/PVP hybrid matrix and PVA/PVP-GnP nanocomposites.

state density and polarization, leading to higher dielectric constant values. These results show that PVA/PVP–GnP composites can be used in supercapacitors and energy storage devices [36].

Dispersion energy parameters

Another approach used to understand the optical behavior of materials and their interaction with light is to determine the dispersion energy parameters. Models such as the Wemple-DiDomenico (W-D) model, in particular, provide very important information about the electronic structure of materials [34, 39]. The W-D model finds extensive applications in fields such as optical material characterization, optical device design (e.g., filters, lenses, waveguides), photovoltaic applications, and dielectric/conductivity studies [26, 39, 44, 54]. It is a method used to investigate how a material's refractive index (n) changes with wavelength in the normal dispersion region, with the spectral dependence of the refractive index [26, 33–35].

E_d reflects the average density of interband optical transitions within the material and is closely related to the chemical bonding structure, charge distribution within the unit cell, and the material's structural order [26, 33, 34]. Additionally, the E_d value also provides information about the type and energy of chemical bonds, indicating changes in structural order and defect density within the material [13, 26, 33, 36, 52].

On the other hand, E_o represents the average band gap energy of the material, also known as the forbidden band energy. This value depends on the composition and structure of the material and provides information about the overall band structure [13, 26, 33–36, 52]. As shown in Fig. 10a, if plotting $(n^2-1)^{-1}$ versus $(h\nu)^2$, reveals a linear relationship between the values. From the slope and intercept of this line, E_o and E_d can be determined.

Additionally, using the W–D model, other optical constants of the material can also be determined, such as the static refractive index (n_∞), static dielectric constant (ε_s), and oscillator strength (f) [33, 36, 37]. The calculated values of E_d, E_o, n_∞, ε_s, f, and E_o/E_g^d for all the composites are presented in Table 2. Firstly, the E_d value decreased from 11.06 for pure PVA/PVP to 8.75 eV for $\phi = 1.19$ vol% GnP and then increased to 12.89 eV for $\phi = 6.16$ vol% GnP. Conversely, E_o decreased from 6.59 for pure PVA/PVP to 5.75 eV for $\phi = 6.16$ vol% GnP. This trend can be attributed to the narrowing of the optical bandgap and an increase in defect density in the nanocomposites [36, 39, 51]. As shown in Table 2, the E_o/E_g^d ratio varies between 1.02 and 1.38. The n_∞ corresponding to the material's refractive index at long wavelengths increased from 1.63 for pure PVA/PVP to 1.80 for $\phi = 6.16$ vol% GnP. Similarly, ε_s increased from 2.67 for pure PVA/PVP to 3.24 for $\phi = 6.16$ vol% GnP. The f values fluctuate and do not show a regular upward or downward trend.

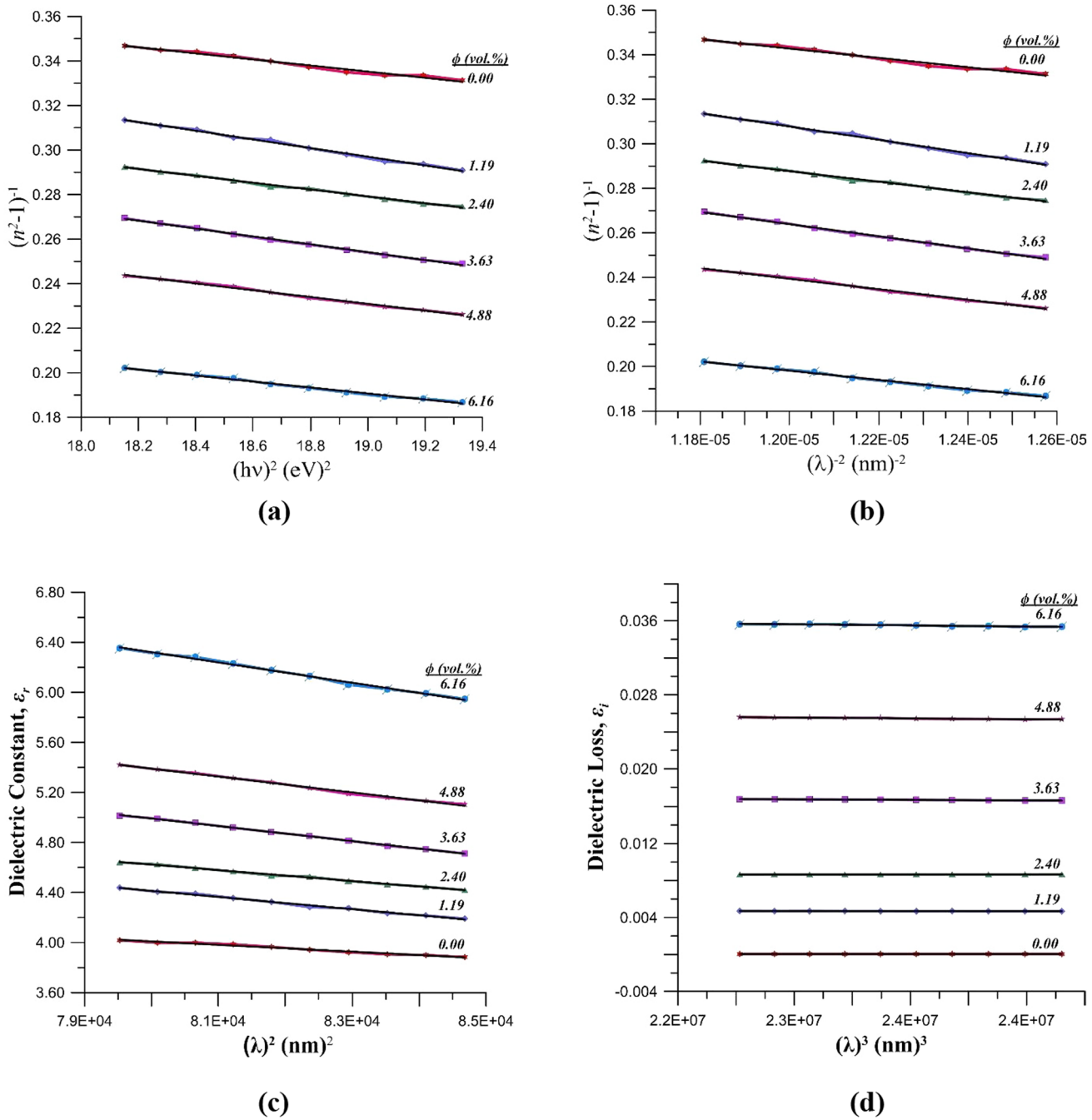

Figure 10 **a** Plots of $(n^2-1)^{-1}$ versus $(h\nu)^2$, **b** Plots of $(n^2-1)^{-1}$ versus $(\lambda)^{-2}$, **c** Plots of (εr) versus $(\lambda)^2$ and **d** Plots of (εi) versus $(\lambda)^3$ of the pure PVA/PVP hybrid matrix and PVA/PVP-GnP nanocomposites.

The Sellmeier oscillator model explains the relationship between the refractive index and wavelength based on oscillations arising from the interaction of light with atoms and molecules within the material [55]. In the one-term Sellmeier model, it is assumed that the largest contribution to the refractive index of the material comes from the oscillator with the lowest energy. Under this assumption, the oscillator equation becomes quite simple. It describes the wavelength dependence of the refractive index using parameters such as the average oscillator strength (S_o) and the average oscillator wavelength (λ_o) [36, 56, 57].

Table 2 E_d, E_o, n_∞, ε_s, f, λ_o, S_o and E_o/E_g^d values of the pure PVA/PVP and PVA/PVP–GnP nanocomposites

ϕ (vol.%)	E_d (eV)	E_o (eV)	n_∞	ε_s	f (eV)^2	λ_o (nm)	S_o (10^{13}) (m^{-2})	E_o/E_g^d
0.00	11.06	6.59	1.63	2.67	72.88	112.09	4.74	1.05
1.19	8.75	5.84	1.58	2.49	51.10	141.55	3.33	1.02
2.40	10.67	6.09	1.65	2.75	64.98	116.12	4.23	1.08
3.63	9.80	5.77	1.64	2.69	56.54	126.54	3.63	1.04
4.88	11.16	5.83	1.70	2.91	65.06	111.00	4.24	1.06
6.16	12.89	5.75	1.80	3.24	74.11	96.18	4.82	1.38

From the slope of the graph plotting $(n^2-1)^{-1}$ against λ^{-2} in Fig. 10b, the value of S_o^{-1} is determined, while the intercept on the Y-axis provides the value of $(S_o\lambda_o^2)^{-1}$. Using these values, the calculated average oscillator strength (S_o) and average oscillator wavelength (λ_o) are given in Table 2. As shown in Table 2, S_o values fluctuate between 3.33×10^{13} and 4.82×10^{13} m^{-2}. In other words, it does not have an increasing and decreasing trend with GnP contribution to PVA/PVP hybrids. Similar to S_o values, λ_o values also fluctuate between 96.18 and 141.5 nm. In the light of these findings, we can say that the addition of GnP to the PVA/PVP hybrid matrix does not cause a significant change in λ_o values.

How the real dielectric constant (ε_r) varies with wavelength (λ) in nanocomposite materials can be analyzed using the Spitzer–Fan model. This model is particularly significant for understanding the behavior of free charge carriers in semiconductors [34, 48, 54]. The model is based on the dielectric response of the material due to the interaction of free charge carriers in the material with the applied electromagnetic field [34, 39].

From the graph of ε_r plotted against λ^2 in Fig. 10c, the values of ε_l and N/m^* were obtained and are presented in Table 3. Table 3 demonstrates that both the ε_l and N/m^* values exhibit an almost regular increase with the addition of GnP to the PVA/PVP hybrid structure. For pure PVA/PVP, $\varepsilon_l=6.19$ and $N/m^*=3.32\times10^{58}$ kg m^{-3}, which increase to $\varepsilon_l=12.84$ and $N/m^*=9.92\times10^{58}$ kg m^{-3}, for $\phi=6.16$ vol% GnP. The increase in ε_l and N/m^* values is associated with an increase in the number of free charge carriers, indicating a greater contribution to the polarization mechanism of the material [34, 47, 48, 54].

One of the models employed in the investigation of electron motion in materials is the Drude free electron model. This model plays a critical role in understanding the collective behavior and interactions of free electrons within a structure. Several key parameters, such as the relaxation time (τ), optical electronic mobility (μ_{opt}), and resonant plasma frequency (ω_p) can be obtained using this model [34, 39].

Figure 10d illustrates the variation of ε_i values for all the composites as a function of λ^3. The relaxation time (τ) can be calculated using the inverse slope of the straight lines in the figure, according to Eq. (21). Additionally, the optical electronic mobility (μ_{opt}) and the resonant plasma frequency (ω_p) can be determined using the Eqs. 22 and 23.

The obtained values of τ, μ_{opt}, and ω_p for all the composites are presented in Table 3. It is seen from the Table 3 that the addition of GnP to the hybrid structure results in a significant decrease in the τ and μ_{opt} values, approaching almost zero, while the ω_p values increase smoothly from 0.96×10^{32} to 2.87×10^{32} s^{-1}. These changes confirm an increase in the number of free charge carriers in the nanocomposites.

Table 3 ω_p, μ_{opt}, τ, ε_l, and N/m^* values of the pure PVA/PVP and PVA/PVP-GnP nanocomposites

ϕ (vol.%)	ω_p(10^{32}) (s^{-1})	μ_{opt} (C s kg^{-1})	τ (10^{-12}) (s)	ε_l	N/m^* (10^{58}) kg m^{-3}
0.00	0.96	9.90	65.27	6.19	3.32
1.19	1.72	0.73	4.84	8.32	5.94
2.40	1.54	0.98	6.47	8.12	5.32
3.63	2.12	0.14	0.90	9.80	7.32
4.88	2.24	0.09	0.57	10.46	7.72
6.16	2.87	0.09	0.59	12.84	9.92

Conclusions

In this study, PVA/PVP–GnP nanocomposite films were successfully synthesized using the solution mixing method, and their structural, electrical, and optical properties were comprehensively investigated. The addition of graphene nanoplatelets (GnPs) in the PVA/PVP structure significantly enhanced the physical characteristics of the composites, making them suitable for advanced technological applications. The electrical conductivity of the nanocomposites increased dramatically due to the presence of GnPs forming conductive pathways within the composite structure. The results of optical investigation showed strong absorption in the UV region and the optical bandgap energy (E_g) decreasing as GnP content increased. These results support the creation of localized energy states and charge transfer complexes. Also, increasing GnP concentrations in the PVA/PVP matrix caused greater disorder and defect levels, and the Urbach energy levels increased accordingly.

The refractive index (n), optical conductivity σ_{opt}, and dielectric constant of the nanocomposites have significantly improved depending on increasing GnP content. This structural transformation indicates that PVA/PVP–GnP nanocomposites hold significant promise for applications in optoelectronic and photonic devices. These findings support the potential use of PVA/PVP–GnP nanocomposites in communication systems and advanced photonic technologies.

The findings of this study underscore the versatility and promising potential of PVA/PVP–GnP nanocomposites for applications in energy storage systems, optoelectronic devices, and advanced optical technologies. Further studies are needed to investigate the long-term stability, scalability, and potential integration of these nanocomposites into commercial applications.

Acknowledgements

Not applicable.

Author contributions

Ömer Bahadır Mergen: Conceptualization, Investigation, Formal analysis, Writing—Original Draft, Visualization. Ertan Arda: Methodology, Resources, Writing—Review and Editing, Supervision, Validation.

Funding

Open access funding provided by the Scientific and Technological Research Council of Türkiye (TÜBİTAK). No funds, grants, or other support was received.

Data availability

The datasets generated during and/or analyzed during the current study are available from the corresponding author on reasonable request.

Declarations

Conflicts of interest Not applicable.

Ethical approval Not applicable.

Supplementary Information The online version contains supplementary material available at https://doi.org/10.1007/s10853-026-13182-0.

Open Access This article is licensed under a Creative Commons Attribution 4.0 International License, which permits use, sharing, adaptation, distribution and reproduction in any medium or format, as long as you give appropriate credit to the original author(s) and the source, provide a link to the Creative Commons licence, and indicate if changes were made. The images or other third party material in this article are included in the article's Creative Commons licence, unless indicated otherwise in a credit line to the material. If material is not included in the article's Creative Commons licence and your intended use is not permitted by statutory regulation or exceeds the permitted use, you will need to obtain permission directly from the copyright holder. To view a copy of

this licence, visit http://creativecommons.org/licenses/by/4.0/.

References

[1] Badawi A, Alharthi SSA (2024) Comprehensive study of the linear/nonlinear optical and electrical features of rGO/Co: TiO_2 nanostructures incorporated PVP/PVA blend. J Inorg Organomet Polym 34:5805–5816. https://doi.org/10.1007/s10904-024-03215-z

[2] Jilani W, Bouzidi A, Zahran HY, Yahia IS (2024) Identifying the functional properties and characterizations of PVA/PVP polymer blends incorporating CdS/ZnO core–shell (ZCS) fillers for optoelectronic applications. J Mater Sci: Mater Electron 35:444. https://doi.org/10.1007/s10854-024-12188-1

[3] Alsaif NAM, Atta A, Abdeltwab E, Abdel-Hamid MM (2024) Synthesis, structural characterization, and optical properties of PVA/MnO_2 materials for optoelectronics applications. Macromol Res 32:35–44. https://doi.org/10.1007/s13233-023-00212-y

[4] Mohammed MI, Zahran HY, Zyoud SH, Shahwan M, Aydin C, Yahia IS, Abdelhameed D (2025) Effects of $Tb(NO_3)_3$ salt on the structural characteristics, optical, and radiation shielding properties of (PVA-PVP- PEG) polymeric composite films. J Polym Res 32:27. https://doi.org/10.1007/s10965-024-04219-6

[5] Farrage NM, Teleb NH, Abd El-Ghany WA (2024) Investigation of the structural and optical properties of Sb_2S_3/PVA/PVP nanocomposites blended sheets for optoelectronic applications. Opt Quant Electron 56:488. https://doi.org/10.1007/s11082-023-06117-5

[6] El-naggar AM, Heiba ZK, Mohamed MB, Kamal AM (2024) Modifying structural, optical, and electrical features of PVA/CMC/PVP blend doped with $ZnWO_4$ and TPAI. J Inorg Organomet Polym 34:3957–3970. https://doi.org/10.1007/s10904-024-03099-z

[7] Soliman TS, Abdel-Salam AI, Morsy M, Matar HA, Khalid A (2024) Structural, optical, and morphological evaluation of PVA/Bi-Ni oxide-rGO nanocomposite casted films for optical devices applications. Phys Scr 99:085985. https://doi.org/10.1088/1402-4896/ad63da

[8] Alziyadi MO, Alruwaili A, Said AMB, Shalaby MS (2025) Investigation of the structural, optical dispersion, and optoelectrical characteristics of PVA/PVP/V_2O_5 nanocomposites for optoelectronic devices. Appl Phys A 131:53. https://doi.org/10.1007/s00339-024-08195-y

[9] Alzahrani HS, Al-Sulami AI, Alsulami QA, Rajeh A (2022) A systematic study of structural, conductivity, linear, and nonlinear optical properties of PEO/PVA-MWCNTs/ZnO nanocomposites films for optoelectronic applications. Opt Mater 133:112900. https://doi.org/10.1016/j.optmat.2022.112900

[10] Choudhary S, Sengwa RJ (2018) ZnO nanoparticles dispersed PVA–PVP blend matrix based high performance flexible nanodielectrics for multifunctional microelectronic devices. Curr Appl Phys 18:1041–1058. https://doi.org/10.1016/j.cap.2018.05.023

[11] Rajesh K, Crasta V, Rithin Kumar NB, Gananatha S, Sangappa Y, Jyothi K, Vijeth H (2020) Effect of MoO_3 nanofiller on structural, optical, mechanical, dielectric and thermal properties of PVA/PVP blend. Mater Res Innov 24:270–278. https://doi.org/10.1080/14328917.2019.1653558

[12] Hemalatha K, Somashekarappa H, Somashekar R (2015) Micro-structure, AC conductivity and spectroscopic studies of cupric sulphate doped PVA/PVP polymer composites. AMPC 5:408–418. https://doi.org/10.4236/ampc.2015.510041

[13] Veena G, Lobo B (2019) Dispersive parameters of oxidized PVA-PVP blend films. Turk J Phys 43:337–354. https://doi.org/10.3906/fiz-1808-21

[14] Heiba ZK, Mohamed MB, Ahmed SI, Alhazime AA (2021) Tailoring the optical properties of PVA/PVP blend by doping with Cu/MnS nanoparticles. J Vinyl Addit Technol 27:410–418. https://doi.org/10.1002/vnl.21815

[15] Mergen ÖB (2023) Farklı Karbon Dolgular İçeren Kitosan Filmlerin Elektrik ve Optik Özelliklerinin İncelenmesi. SDU J Nat Appl Sci 27:485–494. https://doi.org/10.19113/sdufenbed.1311689

[16] Husain MSB, Gupta A, Alashwal BY, Sharma S (2018) Synthesis of PVA/PVP based hydrogel for biomedical applications: a review. Energy Source Part A 40:2388–2393. https://doi.org/10.1080/15567036.2018.1495786

[17] Tommalieh MJ, Awwad NS, Ibrahium HA, Menazea AA (2021) Characterization and electrical enhancement of PVP/PVA matrix doped by gold nanoparticles prepared by laser ablation. Radiat Phys Chem 179:109195. https://doi.org/10.1016/j.radphyschem.2020.109195

[18] Abdolrahimi M, Seifi M, Ramezanzadeh MH (2018) Study the effect of acetic acid on structural, optical and mechanical properties of PVA/chitosan/MWCNT films. Chin J Phys 56:221–230. https://doi.org/10.1016/j.cjph.2017.12.018

[19] Abdelrazek EM, Elashmawi IS, El-khodary A, Yassin A (2010) Structural, optical, thermal and electrical studies on PVA/PVP blends filled with lithium bromide. Curr Appl Phys 10:607–613. https://doi.org/10.1016/j.cap.2009.08.005

[20] Dhatarwal P, Sengwa RJ (2021) Investigation on the optical properties of (PVP/PVA)/Al_2O_3 nanocomposite films for green disposable optoelectronics. Phys B: Condens Matter 613:412989. https://doi.org/10.1016/j.physb.2021.412989

[21] Zidan HM, Abdelrazek EM, Abdelghany AM, Tarabiah AE (2019) Characterization and some physical studies of PVA/PVP filled with MWCNTs. J Mater Res Technol 8:904–913. https://doi.org/10.1016/j.jmrt.2018.04.023

[22] Deghiedy NM, El-Sayed SM (2020) Evaluation of the structural and optical characters of PVA/PVP blended films. Opt Mater 100:109667. https://doi.org/10.1016/j.optmat.2020.109667

[23] Al-Saleh MH, Jawad SA (2016) Graphene nanoplatelet-polystyrene nanocomposite: dielectric and charge storage behaviors. J Electron Mater 45:3532–3539. https://doi.org/10.1007/s11664-016-4505-6

[24] Hussin N, Ibrahim MH, Ahmad F, Yahaya H, Harun SW (2017) Graphene nanoplatelets (GnP)-PVA based passive saturable absorber. TELKOMNIKA 15:814–819. https://doi.org/10.12928/TELKOMNIKA.v15i2.6126

[25] Mergen ÖB, Arda E, Evingür GA, Öztürk ÖK, Pietsch U (2024) Graphene nanoplatelet and multiwalled carbon nanotube doping effect on the structural and physical properties of polyvinyl alcohol composites. J Macromol Sci B 63:161–184. https://doi.org/10.1080/00222348.2023.2257555

[26] Mohamed MB, El-naggar AM, Heiba ZK, Kamal AM (2024) Modifications in the structural, optical, and dielectric properties of PVA/PVP/PEG blend by incorporation of PANi/$ZnWO_4$ nanohybrid for optoelectronic and energy storage devices. Opt Mater 149:115047. https://doi.org/10.1016/j.optmat.2024.115047

[27] Al-Muntaser AA, Pashameah RA, Alzahrani E, AlSubhi SA, Hameed ST, Morsi MA (2023) Graphene nanoplatelets/TiO_2 hybrid nanofiller boosted PVA/CMC blend based high performance nanocomposites for flexible energy storage applications. J Polym Environ 31:2534–2548. https://doi.org/10.1007/s10924-022-02748-z

[28] Sabur DA, Hashim A, Habeeb MA (2023) Fabrication and exploration of the structural and optical properties of Sb_2O_3-GO nanostructures doped PMMA-PC for photodegradation of pollutant dyes. Opt Quant Electron 55:457. https://doi.org/10.1007/s11082-023-04726-8

[29] Anwar SR, Ahmed KK, Ezat GS, Jamal SJ, Osman SS, Arif RJ, Muheddin DQ, Aziz SB (2023) Optical and microscopic characterizations of polyethylene oxides (PEO) doped with nickel nitrate ($NiNO_3$) transition metal salt. Opt Mater 145:114435. https://doi.org/10.1016/j.optmat.2023.114435

[30] Mergen ÖB, Arda E (2023) Electrical, optical and dielectric properties of polyvinylpyrrolidone/graphene nanoplatelet nanocomposites. Opt Mater 139:113823. https://doi.org/10.1016/j.optmat.2023.113823

[31] Al-Harbi N, Atta A, Henaish AMA, Rabia M, Abdelhamied MM (2023) Structural characterization and linear/nonlinear optical behavior of polyaniline/cellulose acetate composite films. J Mater Sci: Mater Electron 34:1215. https://doi.org/10.1007/s10854-023-10598-1

[32] Mergen ÖB, Arda E (2023) Determination of electrical and optical behaviors of carboxymethyl cellulose/graphene nanocomposites. J Mater Sci: Mater Electron 34:1719. https://doi.org/10.1007/s10854-023-11152-9

[33] Mamand DM, Ahmed BY, Aziz DM, Hama PO, Mohammed PA, Abdalkarim KA, Muhammad DS, Hussein AM, Hussen SA, Aziz SB, Hassan J (2025) Advanced spectroscopic approach for exploring the structural, optical, and electronic properties in dye-functionalized chitosan biopolymers. Spectrochim Acta A Mol Biomol Spectrosc 329:125485. https://doi.org/10.1016/j.saa.2024.125485

[34] Ahmed KK, Aziz SB, Abdulwahid RT, Hussen SA, Brza MA (2022) Green synthesized Al-metal complex to reduce the crystalline phase and improve the optical properties of CS based polymer blends. Opt Mater 134:113112. https://doi.org/10.1016/j.optmat.2022.113112

[35] Hassanien AS, El Radaf IM (2020) Optical characterizations of quaternary Cu_2MnSnS_4 thin films: novel synthesis process of film samples by spray pyrolysis technique. Physica B Condens Matter 585:412110. https://doi.org/10.1016/j.physb.2020.412110

[36] Badawi A, Alharthi SS (2023) Enhancement of the optical and electrical performance of PVA/MWCNTs blend via Cu/ZnS nanoparticles doping for flexible eco-friendly applications. Appl Phys A 129:372. https://doi.org/10.1007/s00339-023-06640-y

[37] El Radaf IM (2020) Structural, optoelectrical, linear, and nonlinear optical characterizations of the $Cu_2ZnGeSe_4$ thin films. J Mater Sci: Mater Electron 31:3228–3237. https://doi.org/10.1007/s10854-020-02871-4

[38] Hameed TA, Mohamed F, Turky G, Salama A (2022) Carboxymethylcellulose/polyvinylpyrrolidone filled with Al-doped ZnO nanoparticles as a promising film for optoelectronic applications. Opt Mater 134:113097. https://doi.org/10.1016/j.optmat.2022.113097

[39] Darwesh AH, Mohammed PA, Mamand SM, Hussen SA, Aziz SB, Brza MA, Abdullah RM, Karim WO (2023) Investigation of structural and optical characteristics of biopolymer composites based on polyvinyl alcohol inserted with PbS nanoparticles. Coatings 13:578. https://doi.org/10.3390/coatings13030578

[40] Ali FM (2019) Structural and optical characterization of [(PVA:PVP)-Cu^{2+}] composite films for promising semiconducting polymer devices. J Mol Struct 1189:352–359. https://doi.org/10.1016/j.molstruc.2019.04.014

[41] Mergen ÖB, Arda E (2020) Determination of optical band gap energies of CS/MWCNT bio-nanocomposites by Tauc and ASF methods. Synth Met 269:116539. https://doi.org/10.1016/j.synthmet.2020.116539

[42] Mergen ÖB (2021) Effect of MWCNT addition on the optical band gap of PVA/CS transient biocomposites. J Compos Mater 55:4347–4359. https://doi.org/10.1177/00219983211037050

[43] Heiba ZK, El-naggar AM, Kamal AM, Aldhafiri AM, Mohamed MB (2023) Influence of polyaniline on the structural, linear/nonlinear optical, and dielectric characteristics of poly(vinyl chloride/poly (ethylene oxide)) blends. J Macromol Sci B 63:343–360. https://doi.org/10.1080/00222348.2023.2270269

[44] Aziz DM, Mohammed SJ, Mohammed PA, Al-Zangana S, Aziz SB, Muhammad DS, Abdulwahid RT, Darwesh AHA, Hussein SA (2025) Spectroscopic study of wemple-didomenico empirical formula and Tauc's model to determine the optical band gap of dye-doped polymer based on chitosan: common poppy dye as a novel approach to reduce the optical band gap of biopolymer. Spectrochim Acta A Mol Biomol Spectrosc 325:125142. https://doi.org/10.1016/j.saa.2024.125142

[45] Mohammed MI, Yahia IS (2022) Towards multifunctional applications of fullerene-filled (PVA-PEG) polymeric nanocomposite films: structural, optical, and electrical properties. Phys Scr 97:065813. https://doi.org/10.1088/1402-4896/ac6d1e

[46] Mergen ÖB, Arda E (2026) Comprehensive investigation of linear and nonlinear optical properties and tunable band gaps in CS/PVP-GnP nanocomposites. Mater Res Expr 13:025002. https://doi.org/10.1088/2053-1591/ae3a46

[47] El-naggar AM, Heiba ZK, Kamal AM, Abd-Elkader OH, Abdellatief M, Mohamed MB (2023) PVC polymer/ZnO/NiO/Co_3O_4 nanocomposites: Toward improved optical properties. J Vinyl Addit Technol 30:44–58. https://doi.org/10.1002/vnl.22028

[48] El Radaf M (2019) Structural, optical, optoelectrical and photovoltaic properties of the thermally evaporated Sb_2Se_3 thin films. Appl Phys A 125:832. https://doi.org/10.1007/s00339-019-3114-7

[49] Mohamed F, Sharmoukh W, Youssef AM, Hameed TA (2022) Structural, morphological, optical, and dielectric properties of PVA-PVP filled with zinc oxide aluminum-graphene oxide composite for promising applications. Polym Adv Technol 33:1009–1020. https://doi.org/10.1002/pat.5575

[50] El-naggar AM, Heiba ZK, Kamal AM, Alzahrani KE, Abd-Elkader OH, Mohamed MB (2023) Impact of natural melanin doping on the structural, optical and dielectric characteristics of the PVP/CMC blend. J Taibah Univ Sci 17:2190731. https://doi.org/10.1080/16583655.2023.2190731

[51] Heiba ZK, Kamal AM, El-naggar AM, Mohamed MB, Abdel-Kader MH, Alharby T (2023) Reinforcement of linear/nonlinear optical and dielectric characteristics of PVC/PEG blend based on CeO_2/TBAI filler. Inorg Chem Commun 158:111624. https://doi.org/10.1016/j.inoche.2023.111624

[52] Atta A, Abdeltwab E, Negm H, Rabia M, Abdelhamied MM (2023) Fabrication of polypyrrole/graphene oxide polymer nanocomposites and evaluation of their optical behavior for optoelectronic applications. J Inorg Organomet Polym 33:4083–4095. https://doi.org/10.1007/s10904-023-02643-7

[53] El Radaf IM, Al-Zahrani HYS, Hassanien AS (2020) Novel synthesis, structural, linear and nonlinear optical properties of p-type kesterite nanosized Cu_2MnGeS_4 thin films. J Mater Sci: Mater Electron 31:8336–8348. https://doi.org/10.1007/s10854-020-03369-9

[54] Muhammad DS, Aziz DM, Aziz SB (2025) The impact of green chemistry to synthesize PVA/cobalt metal complexes (CoMCs) composites with enhanced optical behavior. Opt Mater 158:116448. https://doi.org/10.1016/j.optmat.2024.116448

[55] Farag AAM, Yahia IS, Yakuphanoglu F, Kandaz M, Farooq WA (2012) Optical properties and the dispersion parameters of new zinc phthalocyanine benzofuran derivative prepared by non-vacuum spin coating technique. Opt Commun 285:3122–3127. https://doi.org/10.1016/j.optcom.2012.02.061

[56] Saini I, Sharma A, Dhiman R, Aggarwal S, Ram S, Sharma PK (2017) Grafted SiC nanocrystals: for enhanced optical, electrical and mechanical properties of polyvinyl alcohol. J Alloys Compd 714:172–180. https://doi.org/10.1016/j.jallcom.2017.04.183

[57] Ghazy AR, Al-Hossainy AF, El-Sheekh MM, Makhlof MEM (2023) Investigating the differences in structure, morphology, optical properties, laser photoluminescence and dielectric properties for chitosan-doped commercial and polycladia myrica mediated ZnO nanoparticles films combined with TD-DFT simulations. Algal Res 71:103076. https://doi.org/10.1016/j.algal.2023.103076

Publisher's Note Springer Nature remains neutral with regard to jurisdictional claims in published maps and institutional affiliations.